Hindawi Publishing Corporation
Journal of Nanomaterials
Volume 2015, Article ID 678929, 8 pages
http://dx.doi.org/10.1155/2015/678929

Research Article

Effects of Preparation Conditions on the $CuInS_2$ Films Prepared by One-Step Electrodeposition Method

Rongfeng Guan,[1] Liu Cao,[2] Qian Sun,[1] and Yuebin Cao[1,3]

[1]*Key Laboratory for Advanced Technology in Environmental Protection of Jiangsu, Yancheng Institute of Technology, Jiangsu 224051, China*
[2]*Beijing Water Science Technology Institute, Beijing 100044, China*
[3]*Department of Chemical Engineering, Hanyang University, 55 Hanyangdaehak-ro, Sangnok-gu, Ansan, Gyeonggi-do 426-791, Republic of Korea*

Correspondence should be addressed to Yuebin Cao; hxxcyb@gmail.com

Received 17 April 2015; Revised 23 August 2015; Accepted 24 August 2015

Academic Editor: Meiyong Liao

$CuInS_2$ thin films were prepared onto indium tin oxide (ITO) substrates by sulfurization of electrodeposited $Cu_xIn_yS_z$ precursor films under S atmosphere. The influences of deposition potential, Cu^{2+}/In^{3+} ratio, sulfurization temperature, and sulfur content on the $CuInS_2$ thin films were investigated. Phases and structures were characterized by powder X-ray diffraction and Raman spectroscopy; surface morphology was characterized by Scanning Electron Microscopy; optical and electrical properties were characterized by UV-Vis absorption and Mott-Schottky curves, respectively. As a result, the optimal well-crystallized $CuInS_2$ films preparation parameters were determined to be deposition potential of −0.8 V, Cu^{2+}/In^{3+} ratio of 1.4, sulfur content of 1 g, and the sulfurization temperature of 550°C for 1 h; $CuInS_2$ thin films prepared by one-step electrodeposition present the p-type semiconductor, with thickness about 4-5 μm and their optical band gaps in the range of 1.53~1.55 eV.

1. Introduction

$CuInS_2$ is a promising material as absorber layer in photovoltaic devices owing to its direct band gap of about 1.5 eV and a high absorption coefficient, 10^5 cm^{-1} [1–3]. In addition, $CuInS_2$ is of particular interest for being environmentally friendly and cost-effective when compared to $CuInSe_2$ where the toxic and costly Se existed. Until now, the conversion efficiency of about 13% for $CuInS_2$-based solar cells has been achieved [4]. However, the value is still far below its theoretical value of 32% [5], which is mainly influenced by the quality of $CuInS_2$ film.

Preparation methods of $CuInS_2$ film mainly include sputtering [6], evaporation [7], spray pyrolysis [8, 9], chemical bath deposition [10], and electrodeposition [11–16]. Among these methods, sputtering and evaporation are two main methods for industrial production [7, 17–20]. However, expensive equipment is necessary for providing vacuum environment in the two methods, which limit their use in the production of large-area $CuInS_2$ films. Electrodeposition method has been shown to be desirable because of its advantages of low equipment cost, scalability, and manufacturability of large-area thin films. Recently, a high efficient solar cell based on electrodeposited $CuInS_2$ films is fabricated, in which the efficiency is already close to that fabricated by vacuum method [21]. There are two routes for electrodeposition method: for the one-step route, copper, indium, and sulfur are deposited simultaneously usually with sodium thiosulfate as sulfur source, metal salts as copper, and indium sources; for the two-step route, Cu-In precursor films are firstly formed by electrodeposition, and then they are sulfurized to $CuInS_2$ films in H_2S or S atmosphere. It seems that one-step route is more simple and environmentally benign, but the obtained $CuInS_2$ films do not always follow the exact stoichiometry of Cu : In : S = 1 : 1 : 2, usually with S deficiency in the films. Besides, easy formation of secondary phases (such as In_2CuO_4, Cu_2O/Cu_2S, CuO/CuS, and In_2S_3) is another disadvantage. Thus, it is still a challenge

to fabricate high-quality $CuInS_2$ thin films by using one-step electrodeposition route.

To solve S deficiency problem in one-step route, a further sulfurization of $Cu_xIn_yS_z$ precursor films by using S powder or H_2S is usually conducted. To reduce the secondary phases, the operation conditions for $CuInS_2$ film fabrication such as electrodeposition potential, concentration of complexing agent, and Cu^{2+}/In^{3+} ratio need to be optimized. Until now, just few studies reported the effects of detailed operation conditions on the properties of $CuInS_2$ films prepared by one-step electrodeposition method [11, 22]. In the present study, $Cu_xIn_yS_z$ precursor films firstly were electrodeposited on ITO substrates, and then they were further sulfurized in S vapor to $CuInS_2$ films. The effects of deposition potential, Cu^{2+}/In^{3+} ratio in the precursor solution, and sulfurization conditions (S content and heat treatment temperature), on the structure, morphology, and optical and electrical properties of the obtained $CuInS_2$ films were investigated in detail.

2. Experimental Section

Firstly, $Cu_xIn_yS_z$ precursor films were grown on ITO glasses in a conventional three-electrode system using a PARSTAT 2273 Potentiostat. The working, counter, and reference electrodes were ITO-coated glass substrates, a platinum plate, and a saturated calomel electrode (SCE), respectively. The FTO substrates with sheet resistance of 15 Ω/square were cut into several pieces (1.5 cm × 2.5 cm) and ultrasonically cleaned in ethanol, deionized water, and acetone for 30 min, respectively. The solution bath contains 12 mM copper(II) chloride ($CuCl_2{\cdot}2H_2O$), 6.7–10 mM indium chloride ($InCl_3{\cdot}4H_2O$), 25 mM sodium thiosulfate ($Na_2S_2O_3{\cdot}5H_2O$), 0.5 mM potassium chloride (KCl), and 0.1 M citric acid ($C_6H_8O_7$). $C_6H_8O_7$ was employed as a complexing agent, and KCl aqueous solution was used as a supporting electrolyte. pH of the bath solutions was adjusted to 6 using diluted ammonia solution. Deposition of the samples was carried out at room temperature for 30 min. Then the electrodeposited $Cu_xIn_yS_z$ precursor films were further sulfurized by S powders at temperatures 400–550°C in a self-made sealed tubular furnace under the protection of Ar atmosphere.

Phases and crystal structures of the thin films were characterized by X-ray diffraction (XRD), with a German Bruker AXS D8 advanced diffractometer, and Cu Kα radiation at 40 kV and 40 mA. Raman spectroscopy was measured using an InVia laser confocal Raman spectroscopy system of England Renishaw company. Scanning Electron Microscopy (SEM) was measured using a JEOL JSM-6390 LV microscope. UV-Vis absorption spectrum was measured in the wavelength range of 300~900 nm using UV-2450 UV-visible spectroscopy system. Mott-Schottky curve was measured in a mixed solution of 0.2 M KCl and 0.5 M EDTA with frequency 1 KHz, scan range −0.9 to −0.4 V, and scan rate 3 mV/s.

3. Results and Discussions

3.1. Effects of Deposition Potential. In the one-step electrodeposition method, for depositing Cu-In-S simultaneously, complexing agent for narrowing the redox potentials is needed. It was reported that citric acid can work as the complexing agent for narrowing the redox potentials of Cu^{2+}/Cu and In^{3+}/In [23]. Moreover, citric acid can complex with both Cu^{2+} and In^{3+}, which will prevent the precipitation of metal hydroxide over a wide pH range. We previously studied the effects of citric acid concentrations on the redox properties of Cu^{2+} and In^{3+}, and the optimal concentration was determined to be citric acid:Cu^{2+} 8.5 as we used here.

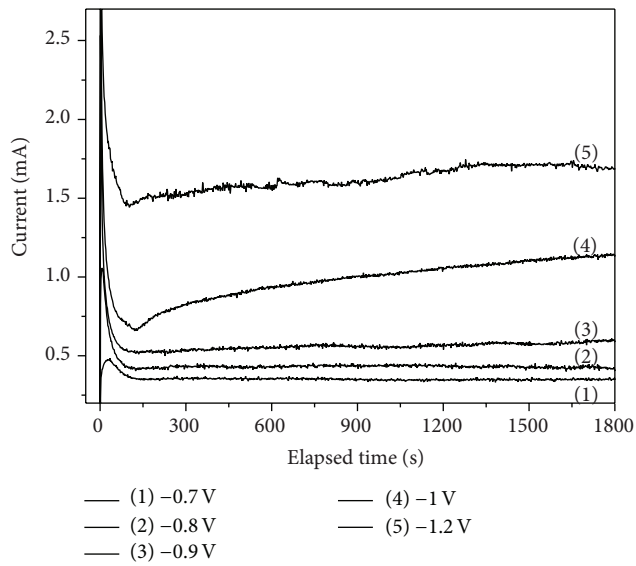

Figure 1: The deposition currents as a function of times at various deposition potentials (−0.7, −0.8, −0.9, −1.0, and −1.2 V).

Figure 1 shows the deposition current as a function of time at various potentials. The deposition current increases with increasing deposition potentials. At any deposition potentials, the current decreases suddenly within initial 2 min, which is the result of concentration gradients developed in the boundary layer close to an electrode surface at short times at initial deposition period [16]. After initial period, the currents at deposition potentials −0.7, −0.8, and −0.9 V are stable, while the currents at potentials −1.0 and −1.2 V increased gradually. It may be because the large deposition rate at high potentials induces the roughness of the electrode surface and deposition area increases and hence the deposition current increases. At −1.0 and −1.2 V, upper layers of $Cu_xIn_yS_z$ films exfoliated during the deposition process due to the weak adhesive force caused by their large deposition rate.

Figure 2 shows the morphology of $Cu_xIn_yS_z$ films deposited at various potentials. All the films are composed of aggregated particles. The films deposited at −0.7 V contain two kinds of particles: secondary particles with large size of around 2-3 μm and primary particles in nanoscale. For the films deposited at −0.8 and −0.9 V, they both are composed of aggregated particles, with a relative uniform particles size distribution at around 1 μm. The films deposited at −0.8 V are more compact and smooth than that deposited at −0.9 V. Thus, the potential −0.8 V is more proper for $Cu_xIn_yS_z$ film deposition. As the upper layers of $Cu_xIn_yS_z$ films deposited

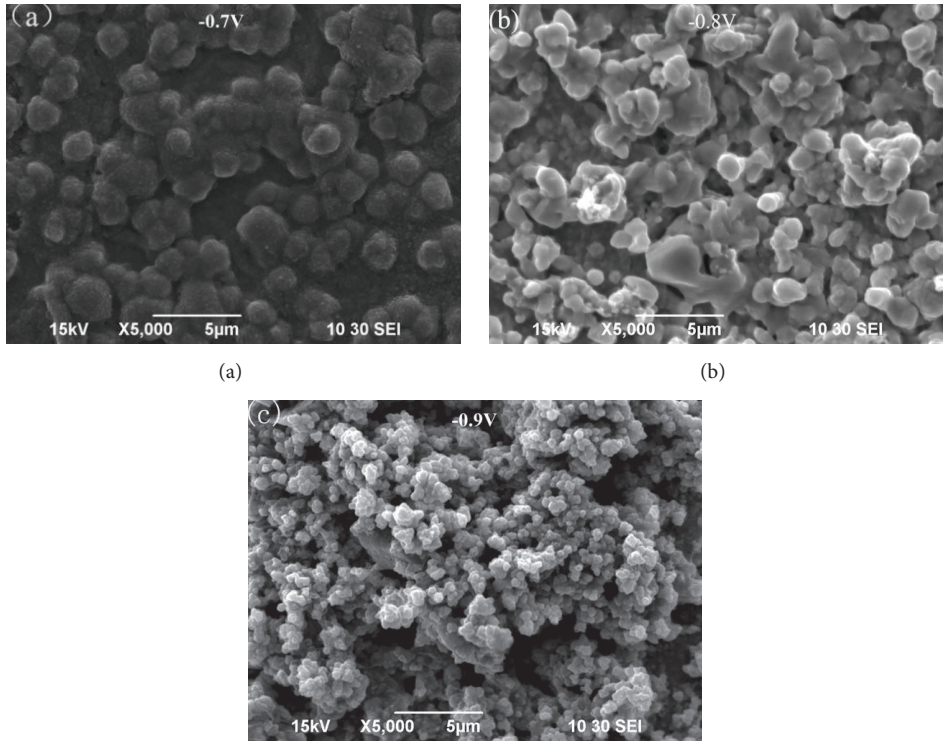

(a) (b)

(c)

Figure 2: SEM images of $CuInS_2$ thin films obtained at deposition potentials −0.7 V (a), −0.8 V (b), and −0.9 V (c).

at −1.0 and −1.2 V are easily exfoliated, their SEM images are not shown here.

3.2. Effects of Sulfurization Parameters. As we mentioned above, $CuInS_2$ films were obtained through one-step electrodeposition method usually with S deficiency. Thus $Cu_xIn_yS_z$ precursor films were further sulfurized, and the effects of sulfurization parameters on $CuInS_2$ film properties were investigated. $Cu_xIn_yS_z$ precursor films were deposited together with a certain amount of S powders in a tube furnace with argon flow during the sulfurization process to avoid air oxidation.

3.2.1. Effects of S Content. Figure 3(a) presents the XRD pattern of $CuInS_2$ films sulfurized at various S contents with sulfurization temperature at 550°C. All $CuInS_2$ films were chalcopyrite structure, with no evidence of other phases, indicating that $CuInS_2$ films were near stoichiometric. All the films show the (112) plane preferred orientation. The peak intensity of $CuInS_2$ films obtained at S contents 0.5 and 1 g is much higher than that obtained at S contents 1.25 and 1.5 g, which indicates the higher crystallization of $CuInS_2$ films sulfurized at low S vapor concentrations.

Raman spectroscopy can be used as a complementary technique to XRD. For $CuInS_2$, there are three structure orders which belong to different space groups, chalcopyrite (CH) structure and CuAu (CA) and CuPt (CP) metastable structures. Because the formation energy of CP structure is high, it is unlikely present in our $CuInS_2$ films. CA structure is undesirable, and it is difficult to identify it using XRD. The Raman A1 mode of CH structure is centered at 290 cm^{-1}, while the Raman A1 mode of metastable CA structure is centered at around 305 cm^{-1}. The chalcopyrite structure therefore can be identified using Raman analysis. Figure 3(b) shows the Raman spectra of $CuInS_2$ films obtained at various S contents. The peak of 287 cm^{-1} appearing at all samples is closer to the A1 mode of CH structure (290 cm^{-1}) [24], indicating the presence of CH structure. Similar to the XRD results, high peaks intensity of $CuInS_2$ films obtained at 0.5 and 1 g indicates their high crystallization. For all the films, there is no evidence for the presence of CA structure whose A1 mode appears at around 305 cm^{-1} [25]. The peak at 470 cm^{-1} for the film obtained at S content 0.5 g can be attributed to $Cu_{2-x}S$. $Cu_{2-x}S$ phase which can be removed by etching the film in KCN solution.

Optical properties of the films were studied by absorption measurements with a UV/visible/NIR spectrophotometer. Figure 4 shows the absorption spectra of $CuInS_2$ films in the range of 400–900 nm. $CuInS_2$ film obtained at S content 1 g exhibits the largest absorption. All the films show a fundamental absorption wavelength at around 800–810 nm, which is similar to the reported values [15]. According to the absorbance spectra, the plots of $(\alpha h\nu)^2$ against $h\nu$ can be obtained, in which α is the absorbance coefficient. The band gap E_g can be estimated from the intercept of the linear portion of the plots on x-axis. Figure 4(b) shows $(\alpha h\nu)^2$ as a

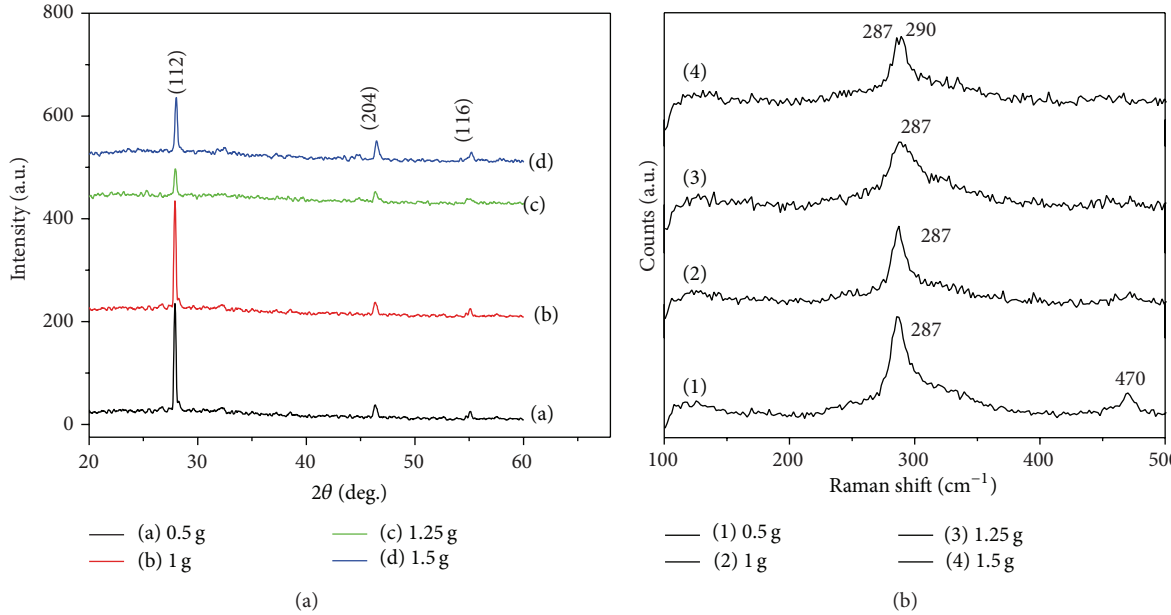

Figure 3: XRD (a) and Raman spectra (b) of $CuInS_2$ films obtained at S contents 0.5, 1, 1.25, and 1.5 g.

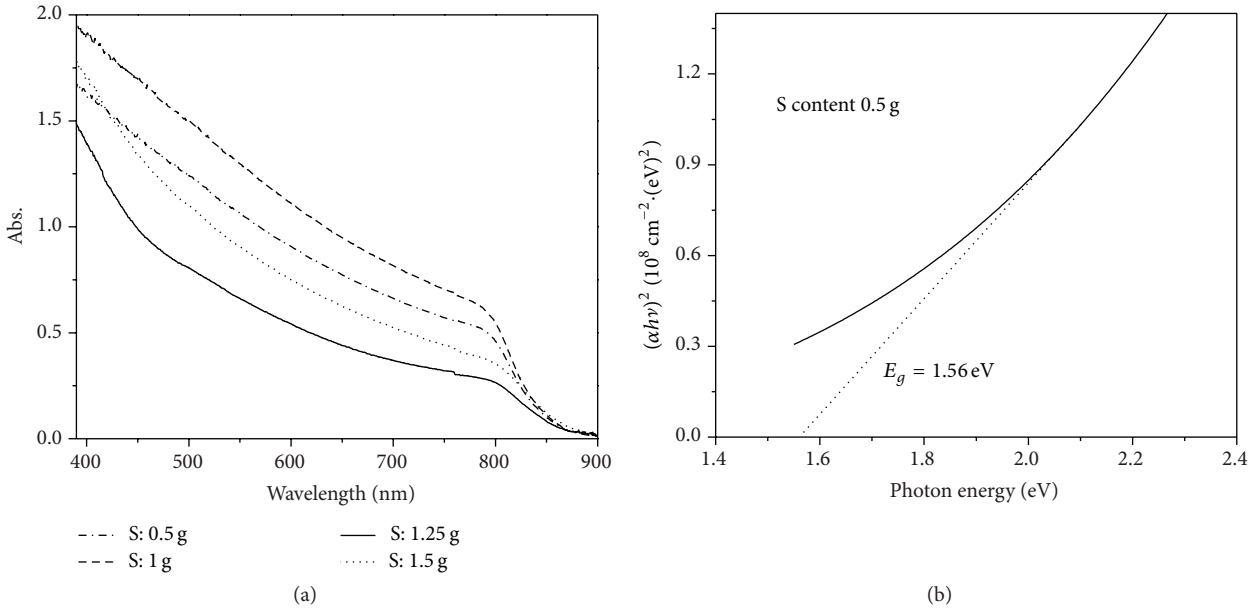

Figure 4: (a) UV-Vis absorption spectra of $CuInS_2$ films obtained at S contents 0.5, 1, 1.25, and 1.5 g; (b) $(\alpha h\nu)^2$ of $CuInS_2$ film obtained at S content 0.5 g as a function of $h\nu$.

function of $h\nu$ for $CuInS_2$ film obtained at S content 0.5 g. E_g of $CuInS_2$ film obtained at S content 0.5 g is determined to be 1.56 eV.

3.2.2. Effects of Annealing Temperature. Figure 5(a) shows the XRD patterns of $CuInS_2$ films heat treated at various temperatures with S content 1 g. When the temperature increased from 400 to 450°C, the intensity of $CuInS_2$ peak at (112) planes greatly enhanced, indicating its enhanced crystallization. When annealing temperature further increased to 500 and 550°C, the peak intensity decreased, which means the crystalization decreased at high temperature. Raman spectra of $CuInS_2$ films annealed at various temperatures are shown in Figure 5(b), in which all $CuInS_2$ films except the one annealed at 550°C contain $Cu_{2-x}S$ phase. From the results of XRD and Raman, it can be concluded that 550°C is a prefferred annealing temperatre for $Cu_xIn_yS_z$ films sulfurazation.

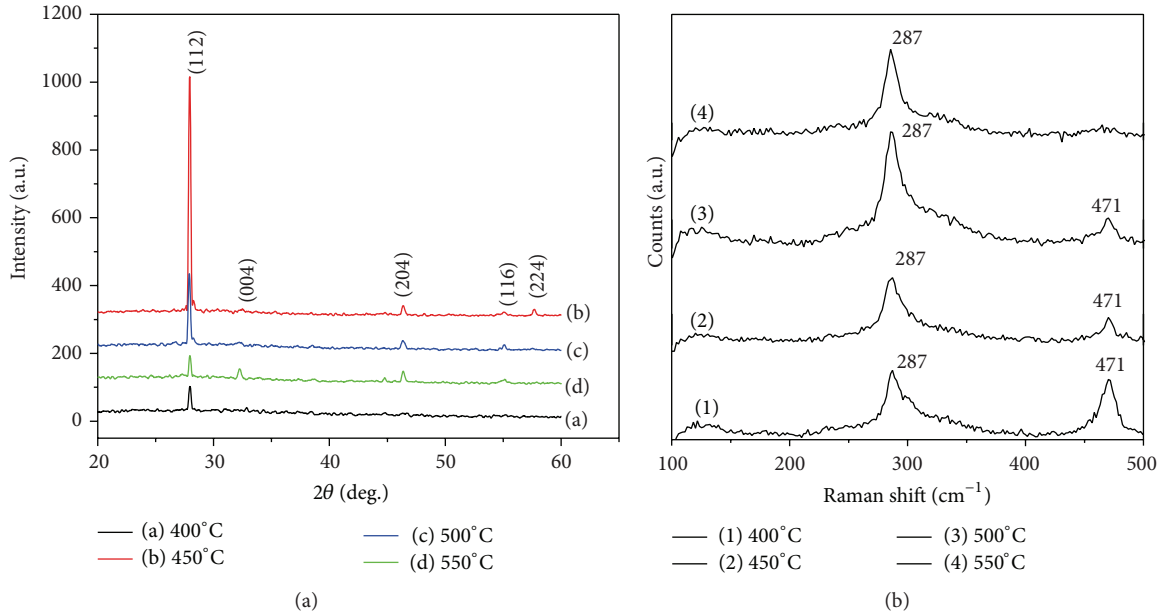

Figure 5: XRD (a) and Raman (b) spectra of $CuInS_2$ films annealed at temperatures 400°C, 450°C, 500°C, and 550°C.

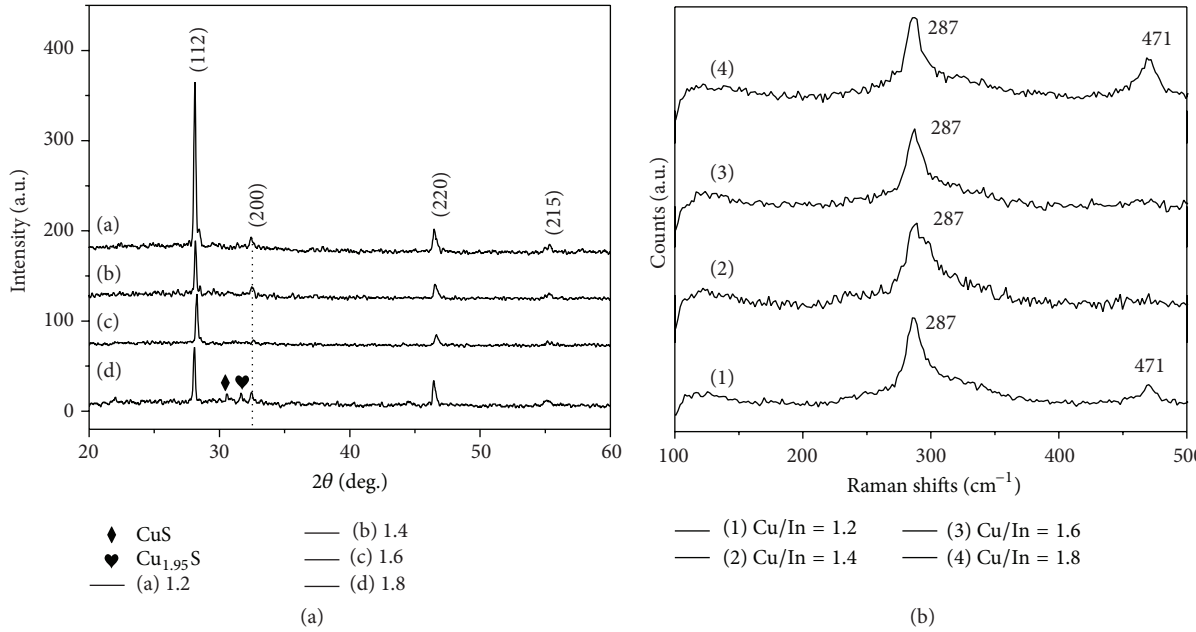

Figure 6: XRD (a) and Raman spectra (b) of $CuInS_2$ films obtained at Cu^{2+}/In^{3+} 1.2, 1.4, 1.6, and 1.8.

3.3. Effects of Cu^{2+}/In^{3+} Ratios. Cu^{2+}/In^{3+} ratio in precursor solution is a crucial parameter in determining the properties of synthesized $CuInS_2$ films. Here, the effects of Cu^{2+}/In^{3+} ratio in solution on $CuInS_2$ film phases, morphologies, and optical properties are investigated. Figure 6(a) shows the XRD patterns of $CuInS_2$ films prepared at various Cu^{2+}/In^{3+} ratios. All the films, except the film obtained at Cu^{2+}/In^{3+} ratio 1.8, are chalcopyrite structure without observable other phases. For $CuInS_2$ film obtained at Cu^{2+}/In^{3+} ratio 1.8, there are other phases including CuS and $Cu_{1.95}S$ as labelled in the (d) curve of Figure 6(a). Raman spectra as shown in Figure 5(b) also indicate that $Cu_{2-x}S$ phase is present in the film obtained at Cu^{2+}/In^{3+} ratio 1.8, as the peak at 471 cm^{-1} which is a typical peak from $Cu_{2-x}S$ existed. From the Raman spectrum, it can be seen that the film obtained at Cu^{2+}/In^{3+} ratio 1.2 also contained $Cu_{2-x}S$, although it was not detected in XRD measurement.

SEM images of $CuInS_2$ films obtained at Cu^{2+}/In^{3+} ratios 1.4 and 1.6 are shown in Figure 7. The plane and cross-sectional images of $CuInS_2$ film obtained at Cu^{2+}/In^{3+} ratios

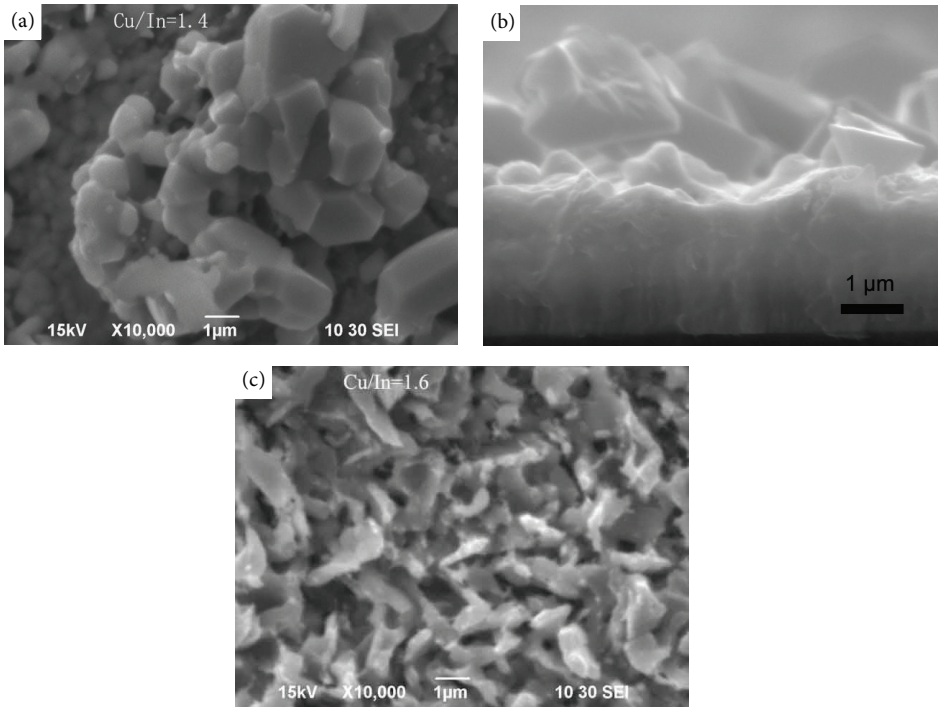

FIGURE 7: SEM images of $CuInS_2$ thin films obtained at Cu^{2+}/In^{3+} ratio 1.4 (a) plane view, (b) cross-section view, and Cu^{2+}/In^{3+} ratio 1.6 (c).

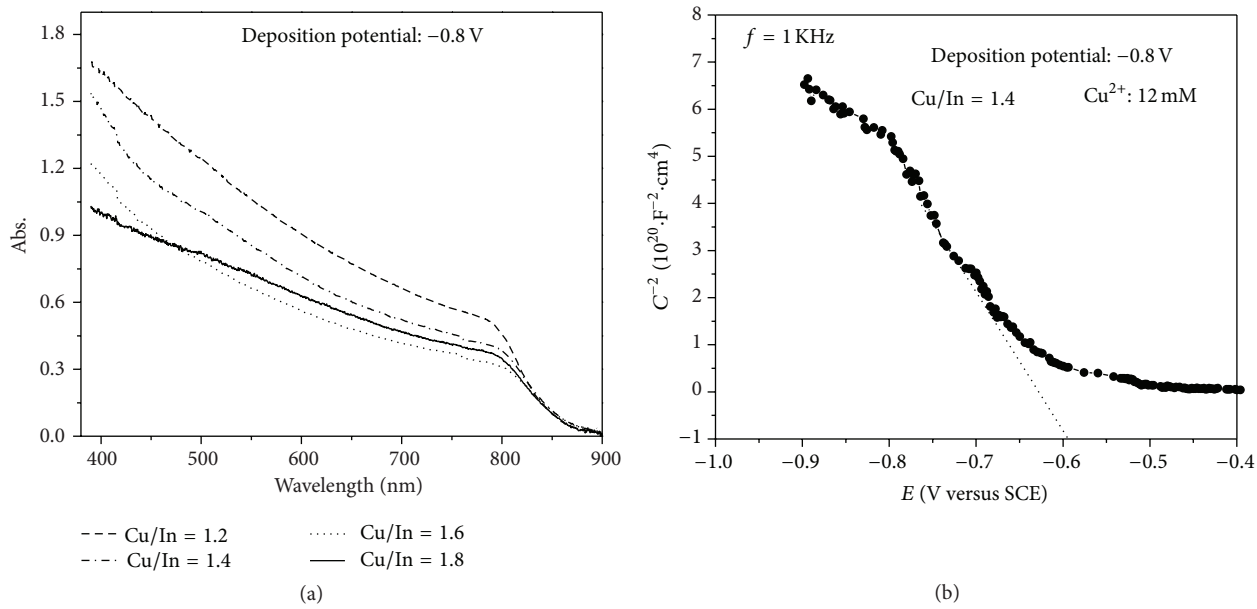

FIGURE 8: (a) UV-Vis absorption spectra of $CuInS_2$ films obtained at various Cu^{2+}/In^{3+} ratios; (b) Mott-Schottky curve of $CuInS_2$ thin films obtained at Cu^{2+}/In^{3+} ratio 1.4.

1.4 indicate that the film can be divided into two layers: the condensed bottom layer with thickness of around 2 μm and the incompact upper layer with large crystals. Large crystals of the upper layer may be caused by the sulfurization process. It can be seen from Figures 7(a) and 7(c) that crystal size of the film obtained at Cu^{2+}/In^{3+} ratio 1.4 is much larger than that obtained at Cu^{2+}/In^{3+} ratio 1.6 and the surface of the film obtained at Cu^{2+}/In^{3+} ratio 1.4 is more condense than that obtained at Cu^{2+}/In^{3+} ratio 1.6. The condensed film and large crystals mean reduced cracks and grain boundaries in the film which will increase photocurrent because the traps for electrons and holes are reduced. Thus, the film obtained at Cu^{2+}/In^{3+} ratio 1.4 has the potential to be an effective absorber layer for solar cells. As there are $Cu_{2-x}S$ phases in

the films obtained at Cu^{2+}/In^{3+} ratio 1.2 and 1.8, we did not show their SEM images here.

In solution-based processes carbon contamination is an important issue for $CuInS_2$ film fabrication. EDS was used to determine the carbon content, and it indicates that the carbon is 3.5 at% in $CuInS_2$ film obtained at Cu^{2+}/In^{3+} ratio 1.4. We estimate that the carbon contamination may come from citrate used in solution.

Figure 8(a) shows the absorption spectra of $CuInS_2$ films obtained at various Cu^{2+}/In^{3+} ratios. $CuInS_2$ film obtained at Cu^{2+}/In^{3+} ratio 1.2 shows the largest absorption; and all the films have a similar fundamental absorption wavelength at around 800–810 nm, caused by their band gaps. Figure 8(b) shows the Mott-Schottky (MS) plots for $CuInS_2$ film obtained at Cu^{2+}/In^{3+} ratio 1.4. It can be determined that the film is p-type semiconductor due to the negative slope of the curve. According to the intercept on the potential axis, the flat band potential is determined to be −0.6 V.

4. Conclusions

$CuInS_2$ films of chalcopyrite structure were prepared by one-step electrodeposition of $Cu_xIn_yS_z$ precursor films, followed by sulfurization. Effects of operation parameters including deposition potential, sulfurization conditions, Cu^{2+}/In^{3+} ratio on the structure, morphology, and optical and electrical properties of the obtained $CuInS_2$ films were studied. Based on the surface morphology, crystallization, phases purity, and optical absorption property, the optimized deposition potential was determined to be −0.8 V, Cu^{2+}/In^{3+} ratio 1.4, sulfur content 1 g, and sulfurization temperature 550°C. The obtained $CuInS_2$ thin films prepared here present p-type semiconductor, with thickness about 4-5 μm and optical band gaps 1.53–1.55 eV.

Conflict of Interests

The authors declare that there is no conflict of interests regarding the publication of this paper.

Acknowledgments

This work was financially supported by the National Natural Science Foundation (21276220), National Key Technology Support Program (no. 2013BAC13B00), and the Key Laboratory for Advanced Technology in Environmental Protection of Jiangsu Province (AE201124).

References

[1] S. M. Hosseinpour-Mashkani, M. Salavati-Niasari, and F. Mohandes, "$CuInS_2$ nanostructures: synthesis, characterization, formation mechanism and solar cell applications," *Journal of Industrial and Engineering Chemistry*, vol. 20, no. 5, pp. 3800–3807, 2014.

[2] B. D. Weil, S. T. Connor, and Y. Cui, "$CuInS_2$ solar cells by air-stable ink rolling," *Journal of the American Chemical Society*, vol. 132, no. 19, pp. 6642–6643, 2010.

[3] J. S. Ward, K. Ramanathan, F. S. Hasoon et al., "A 21·5% efficient $Cu(In,Ga)Se_2$ thin-film concentrator solar cell," *Progress in Photovoltaics: Research and Applications*, vol. 10, no. 1, pp. 41–46, 2002.

[4] H. Goto, Y. Hashimoto, and K. Ito, "Efficient thin film solar cell consisting of $TCO/CdS/CuInS_2/CuGaS_2$ structure," *Thin Solid Films*, vol. 451-452, pp. 552–555, 2004.

[5] T. Nakabayashi, T. Miyazawa, Y. Hashimoto, and K. Ito, "Over 10% efficient $CuInS_2$ solar cell by sulfurization," *Solar Energy Materials & Solar Cells*, vol. 49, no. 1–4, pp. 375–381, 1997.

[6] J. Schulte, S. Brunken, and K. Ellmer, "Nucleation and phase formation during reactive magnetron co-sputtering of $Cu(In,Ga)S_2$ films, investigated by *in situ* EDXRD," *Journal of Crystal Growth*, vol. 384, pp. 114–121, 2013.

[7] P. Rao, S. Kumar, and N. K. Sahoo, "Growth of copper indium sulphide films by thermal evaporation of mixtures of copper sulphide and indium sulphide powders," *Materials Research Bulletin*, vol. 48, no. 8, pp. 2915–2921, 2013.

[8] R. R. Prabhakar, S. S. Pramana, K. R. G. Karthik, C. H. Sow, and K. B. Jinesh, "Ultra-thin conformal deposition of CuInS2 on ZnO nanowires by chemical spray pyrolysis," *Journal of Materials Chemistry*, vol. 22, no. 28, pp. 13965–13968, 2012.

[9] J. C. W. Ho, T. Zhang, K. K. Lee, S. K. Batabyal, A. I. Y. Tok, and L. H. Wong, "Spray pyrolysis of $CuIn(S,Se)_2$ solar cells with 5.9% efficiency: a method to prevent Mo oxidation in ambient atmosphere," *ACS Applied Materials and Interfaces*, vol. 6, no. 9, pp. 6638–6643, 2014.

[10] F. Cui, L. Wang, Z. Xi, Y. Sun, and D. Yang, "Fabrication and characterization of $CuInS_2$ films by chemical bath deposition in acid conditions," *Journal of Materials Science: Materials in Electronics*, vol. 20, no. 7, pp. 609–613, 2009.

[11] L. Lu, Y. Wang, and X. Li, "Influence of processing parameters on the preparation of $CuInS_2$ thin film by one-step electrodeposition as the solar cell absorber," *Surface & Coatings Technology*, vol. 212, pp. 55–60, 2012.

[12] S. M. Lee, S. Ikeda, T. Yagi, T. Harada, A. Ennaoui, and M. Matsumura, "Fabrication of CuInS2 films from electrodeposited Cu/In bilayers: effects of preheat treatment on their structural, photoelectrochemical and solar cell properties," *Physical Chemistry Chemical Physics*, vol. 13, no. 14, pp. 6662–6669, 2011.

[13] X. Xu, F. Wang, J. Liu, and J. Ji, "Effect of potassium hydrogen phthalate ($C_8H_5KO_4$) on the one-step electrodeposition of single-phase $CuInS_2$ thin films from acidic solution," *Electrochimica Acta*, vol. 55, no. 15, pp. 4428–4435, 2010.

[14] K.-W. Cheng and W.-H. Chiang, "Effect of [Cu]/[Cu + In] ratio in the solution bath on the growth and physical properties of $CuInS_2$ film using one-step electrodeposition," *Journal of Electroanalytical Chemistry*, vol. 661, no. 1, pp. 57–65, 2011.

[15] Y.-C. Chen, J.-B. Shi, P.-F. Wu, C.-J. Chen, and S.-Y. Yang, "Synthesis and optical properties of CuInS2 thin films prepared by sulfurization of electrodeposited Cu-In layers," *Crystal Research and Technology*, vol. 47, no. 9, pp. 991–996, 2012.

[16] J. L. Yuan, C. Shao, L. Zheng et al., "Fabrication of $CuInS_2$ thin film by electrodeposition of Cu-In alloy," *Vacuum*, vol. 99, pp. 196–203, 2014.

[17] R. F. Guan, X. X. Wang, and Q. Sun, "Structural and optical properties of $CuInS_2$ thin films prepared by magnetron sputtering and sulfurization heat treatment," *Journal of Nanomaterials*, In press.

[18] R. Cayzac, F. Boulc'h, M. Bendahan, P. Lauque, and P. Knauth, "Direct preparation of crystalline $CuInS_2$ thin films by radiofrequency sputtering," *Materials Science and Engineering B*, vol. 157, no. 1–3, pp. 66–71, 2009.

[19] M. Nie and K. Ellmer, "Growth and morphology of thin $Cu(In,Ga)S_2$ films during reactive magnetron co-sputtering," *Thin Solid Films*, vol. 536, pp. 172–178, 2013.

[20] C.-H. Tsai, D. K. Mishra, C.-Y. Su, and J.-M. Ting, "Effects of sulfurization and Cu/In ratio on the performance of the $CuInS_2$ solar cell," *International Journal of Energy Research*, vol. 38, no. 4, pp. 418–428, 2014.

[21] C. Broussillou, M. Andrieux, M. Herbst-Ghysel et al., "Sulfurization of Cu-In electrodeposited precursors for $CuInS_2$-based solar cells," *Solar Energy Materials and Solar Cells*, vol. 95, no. 1, pp. S13–S17, 2011.

[22] Y. Tang, Y. H. Ng, and R. Amal, "Investigating the preparation parameters during the synthesis of CuInS2 thin film photoelectrodes," in *Proceedings of the International Conference on Nanoscience and Nanotechnology (ICONN '14)*, pp. 7–9, February 2014.

[23] J. Herrero and J. Ortega, "Electrodeposition of Cu-In alloys for preparing $CuInS_2$ thin films," *Solar Energy Materials*, vol. 20, no. 1-2, pp. 53–65, 1990.

[24] J. Álvarez-García, J. Marcos-Ruzafa, A. Pérez-Rodríguez, A. Romano-Rodríguez, J. R. Morante, and R. Scheer, "MicroRaman scattering from polycrystalline $CuInS_2$ films: structural analysis," *Thin Solid Films*, vol. 361, pp. 208–212, 2000.

[25] J. Ạlvarez-García, A. Pérez-Rodríguez, B. Barcones et al., "Polymorphism in $CuInS_2$ epilayers: origin of additional Raman modes," *Applied Physics Letters*, vol. 80, no. 4, pp. 562–564, 2002.